

Use of hyperspectral remote sensing reflectance for detection and assessment of the harmful alga, *Karenia brevis*

Susanne E. Craig, Steven E. Lohrenz, Zhongping Lee, Kevin L. Mahoney, Gary J. Kirkpatrick, Oscar M. Schofield, and Robert G. Steward

We applied two numerical methods to *in situ* hyperspectral measurements of remote sensing reflectance R_{rs} to assess the feasibility of remote detection and monitoring of the toxic dinoflagellate, *Karenia brevis*, which has been shown to exhibit unique absorption properties. First, an existing quasi-analytical algorithm was used to invert remote sensing reflectance spectra, $R_{rs}(\lambda)$, to derive phytoplankton absorption spectra, $a_{\phi}^{Rrs}(\lambda)$. Second, the fourth derivatives of the $a_{\phi}^{Rrs}(\lambda)$ spectra were compared to the fourth derivative of a reference *K. brevis* absorption spectrum by means of a similarity index (SI) analysis. Comparison of reflectance-derived a_{ϕ} with filter pad measured a_{ϕ} found them to agree well ($R^2 = 0.891$; average percentage difference, 22.8%). A strong correlation ($R^2 = 0.743$) between surface cell concentration and the SI was observed, showing the potential utility of SI magnitude as an indicator of bloom strength. A sensitivity analysis conducted to investigate the effects of varying levels of cell concentrations and colored dissolved organic matter (CDOM) on the efficacy of the quasi-analytical algorithm and SI found that $a_{\phi}^{Rrs}(\lambda)$ could not be derived for very low cell concentrations and that, although it is possible to derive $a_{\phi}^{Rrs}(\lambda)$ in the presence of high CDOM concentrations, CDOM levels influence the $a_{\phi}^{Rrs}(\lambda)$ amplitude and shape. Results suggest that detection and mapping of *K. brevis* blooms based on hyperspectral measurements of R_{rs} are feasible. © 2006 Optical Society of America
OCIS codes: 010.4450, 280.0280.

1. Introduction

Harmful algal blooms represent a significant and increasing threat to human health, fisheries, and valuable tourist industries, particularly in coastal waters.¹ The dinoflagellate, *Karenia brevis*, is the organism responsible for red tides off the west coast of

Florida and in many other coastal regions.² *K. brevis* produces the toxin, brevetoxin, which is responsible for neurotoxic shellfish poisoning, marine mammal and fish mortality, and respiratory irritation in humans and other mammals.² Traditional means of detecting *K. brevis* rely primarily on water sampling for laboratory-based cell enumeration, and these direct microscopic observations are time consuming, labor intensive, and temporally and spatially limited.

Researchers have shown that *K. brevis* can be discriminated from other bloom forming species based on analyses of its optical properties.³⁻⁵ Millie *et al.*³ presented the similarity index (SI) analysis⁶ for *K. brevis* identification, where the fourth derivative of the particulate absorption of an unknown sample is compared with the fourth derivative of the particulate absorption spectrum of a monospecific *K. brevis* culture. Results showed that the SI could correctly discern *K. brevis* from a hypothetical mixed phytoplankton assemblage. The reason for the success of this approach lies in the fact that *K. brevis* displays unique absorption peaks at 444 and 469 nm owing to the presence of a photosynthetic pigment, *gyroxanthin diester*.³⁻⁷ Fourth-derivative analysis amplifies minor inflections in the absorption spectrum and so permits resolution of the gyroxanthin-diester absorp-

S. E. Craig (susanne.craig@dal.ca) and S. E. Lohrenz were with the Department of Marine Science, University of Southern Mississippi, Stennis Space Center, 1020 Balch Boulevard, MS 39529 when this research was performed. Z. Lee is with the Naval Research Laboratory, Code 7333, Stennis Space Center, MS 39529.

K. L. Mahoney is with the Naval Oceanographic Office, N35, Stennis Space Center, MS 39529. G. J. Kirkpatrick is with the Mote Marine Laboratory, 1600 Ken Thompson Parkway, Sarasota, Florida 34236. O. M. Schofield is with the Institute of Marine and Coastal Science, Rutgers University, 71 Dudley Road, New Brunswick, New Jersey 08901. R. G. Steward is with the Florida Environmental Research Institute, Suite 101, 4807 Bayshore Boulevard, Tampa, Florida 33611. S. Craig is now with the Centre for Marine Environmental Prediction, Department of Oceanography, Dalhousie University, Halifax B3H 4J1, Canada.

Received 3 November 2005; revised 10 March 2006; accepted 13 March 2006; posted 14 March 2006 (Doc. ID 65728).

0003-6935/06/215414-12\$15.00/0

© 2006 Optical Society of America

tion maxima.⁵ These maxima give *K. brevis* sufficient optical uniqueness to allow discrimination from other species. Kirkpatrick *et al.*⁵ successfully extended this approach to particulate absorption measurements, made *in situ* and continuously, using a liquid waveguide capillary cell, of natural, mixed phytoplankton communities. In addition to demonstrating the utility of the SI analysis for natural phytoplankton communities, Kirkpatrick *et al.*⁵ found that there was a linear relationship between biomass and SI magnitude, potentially permitting rapid determination of bloom magnitudes from *in situ* measurements. Kirkpatrick has further developed the liquid waveguide capillary cell⁸ and has packaged it as the *BreveBuster*.⁹ It is routinely deployed on a variety of platforms, e.g., moorings,⁹ and on low power consumption gliders.¹⁰ However, these methods are limited by the area that they can usefully monitor.

Remote sensing has been proposed as a means of synoptically monitoring, detecting, and characterizing the location and extent of harmful algal blooms^{4,11,12} and is becoming increasingly relied on by researchers and coastal management agencies. Stumpf *et al.*¹³ developed a statistically based approach that combines climatological data and flags for anomalous chlorophyll in Sea-Viewing Wide Field of View Sensor (SeaWiFS) imagery of the west coast of Florida. They defined an anomaly to flag for *K. brevis* as the difference in chlorophyll values between a single image and a 60 day running mean, ending two weeks before the image. A chlorophyll anomaly of $>1 \mu\text{g}^{-1}$, corresponding to a potential bloom of 100 cells ml^{-1} , was considered indicative of *K. brevis*. Since *K. brevis* blooms usually occur in the late summer and early autumn, chlorophyll anomalies detected in this period are likely to indicate *K. brevis* blooms.^{14,15} In an examination of satellite imagery and cell counts of >100 cells ml^{-1} , Stumpf *et al.*¹³ found that chlorophyll anomaly flags accurately identified *K. brevis* bloom and nonbloom events along the west Florida coast 75% of the time, from 1999 to 2001. In a retrospective analysis of this technique, Tomlinson *et al.*¹⁶ found that this method¹³ accurately identified *K. brevis* blooms along the Florida Panhandle, from Tampa Bay to Cape Romano and Key West greater than 83% of the time during the August to April bloom season. It was observed that areas high in colored dissolved and suspended matter were prone to anomalies that falsely identify *K. brevis* blooms, and Tomlinson *et al.*¹⁶ recommended that the technique not be applied in optically complex waters such as the Big Bend of Florida and from Cape Romano to Florida Bay.

Cannizzaro *et al.*¹⁷ have also reported unique optical properties of *K. brevis* based on its characteristically low backscatter-to-absorption ratio. They developed a classification technique for identifying waters dominated by *K. brevis* blooms and demonstrated that the technique could be applied to SeaWiFS imagery. However, the ratio is able to discern b_b/a species differences only in waters with low scattering and colored dissolved organic matter (CDOM).^{13,16}

Despite the detailed studies carried out by these researchers on the use of derivative-similarity index and ocean color techniques for detecting and assessing blooms of *K. brevis*, we are unaware of any systematic exploration of the utility of hyperspectral remote sensing reflectance for this purpose. The research shows that the absorption properties of *K. brevis* are sufficiently unique to allow discrimination from other species; on this basis, we employ a quasi-analytical algorithm developed by Lee *et al.*¹⁸ to derive a phytoplankton absorption spectrum for *K. brevis* blooms from measurements of *in situ* remote sensing reflectance. This algorithm has been shown to perform well in coastal waters¹⁸ and so is appropriate for the waters in which *K. brevis* regularly blooms.² In addition, we compare the fourth derivatives of reflectance-derived absorption coefficients to a fourth derivative of a reference *K. brevis* spectrum by means of SI analysis^{3,5,19,20} and examine the relationship of this index to surface cell counts. It is our assertion that the combination of these two numerical methods provides an optical means to synoptically detect and, to some extent, provide a quantitative estimate of *K. brevis* cell concentrations.

2. Methods

A. Hyperspectral Remote Sensing, $R_{rs}(\lambda)$, Measurements
Hyperspectral measurements of remote sensing reflectance R_{rs} (see Table 1 for a full list of symbols and definitions) were made aboard the ship RV Suncoaster in waters off the west coast of Florida. These cruises were part of the Ecology and Oceanography of Harmful Algal Blooms (ECOHAB) Florida project, which was designed to predict the development, growth, and transport of *K. brevis* on the west Florida shelf and in adjacent waters. Measurements were taken during three years—during 9–14 September 1999, 20–25 October 2001, and 3–7 November 2003—and covered areas around Tampa Bay and Charlotte Harbor (Fig. 1). For the 1999 and 2003 cruises, measurements to determine hyperspectral R_{rs} were made with a SPECTRIX—a custom-built, hand-held spectroradiometer with 512 channels and a wavelength range of 350–900 nm. Multiple spectra of upwelling radiance above the surface, L_u , and downwelling sky radiance, L_{sky} , were measured at each station. L_u and L_{sky} measurements were made at 30° from nadir and 30° from zenith, respectively, and 90° from the solar plane. Total remote sensing reflectance T_{rs} (i.e., the sum of the water leaving and reflected radiances), and sky input S_{rs} were calculated for each SPECTRIX scan by use of

$$T_{rs} = \frac{L_u R_G}{L_G \pi}, \quad S_{rs} = \frac{L_{sky} R_G}{L_G \pi}, \quad (1)$$

where L_G is the radiance reflected from a diffuse reflector (Spectralon) and R_G is its reflectance.

Following the method of Lee *et al.*,²¹ averages of T_{rs} and S_{rs} were taken to reduce the influence of an un-

Table 1. List of Symbols Used in This Paper

Symbol	Description	Unit
a	Total absorption coefficient, $a = a_w + a_\varphi + a_g$	m^{-1}
a^*	Chlorophyll a specific absorption	$m^2 mg^{-1}$
a_φ	Absorption coefficient of phytoplankton pigments	m^{-1}
a_φ^{pad}	Absorption coefficient of phytoplankton pigments determined from filter pad measurements	m^{-1}
a_φ^{Rrs}	Reflectance-derived absorption coefficient of phytoplankton pigments	m^{-1}
$a_\varphi^{HLI Rrs}$	Reflectance-derived absorption coefficient of phytoplankton pigments from scenario I Hydrolight simulations	m^{-1}
$a_\varphi^{HLII Rrs}$	Reflectance-derived absorption coefficient of phytoplankton pigments from scenario II Hydrolight simulations	m^{-1}
a_φ^{ref}	Reference absorption coefficient of <i>K. brevis</i> culture	m^{-1}
a_g	Absorption coefficient of CDOM and detritus	m^{-1}
a_{CDOM}	Absorption coefficient of CDOM	m^{-1}
b	Total scattering coefficient	m^{-1}
b_b	Total backscattering coefficient, $b_b = b_{bw} + b_{bp}$	m^{-1}
b_{bp}	Backscattering coefficient of suspended particles	m^{-1}
b_{bw}	Backscattering coefficient of pure seawater	m^{-1}
b_w	Scattering coefficient of pure seawater	m^{-1}
c	Beam attenuation coefficient	m^{-1}
E_d	Downwelling irradiance	$W m^{-2}$
F	Fresnel reflectance	Dimensionless
γ	CDOM spectral slope	nm^{-1}
λ_0	Reference wavelength	nm
L_G	Radiance reflected from a diffuse reflector	$W m^{-2} sr^{-1} nm^{-1}$
L_{sky}	Downwelling sky radiance	$W m^{-2} sr^{-1} nm^{-1}$
L_u	Above-surface upwelling radiance	$W m^{-2} sr^{-1} nm^{-1}$
L_w	Water-leaving radiance	$W m^{-2} sr^{-1} nm^{-1}$
R_G	Reflectance from a diffuse reflector	sr^{-1}
R_{rs}	Above-surface remote sensing reflectance	sr^{-1}
r_{rs}	Below-surface remote sensing reflectance	sr^{-1}
S_{QAA}	Spectral slope of detritus and CDOM used in the QAA	nm^{-1}
S_{rs}	Sky contribution to remote sensing reflectance	sr^{-1}
T_{rs}	Total remote sensing reflectance	sr^{-1}
ζ	Ratio of $a_\varphi(410)/a_\varphi(440)$	Dimensionless

even sea surface. Remote sensing reflectance R_{rs} was calculated as follows:

$$R_{rs}(\lambda) = T_{rs}(\lambda) - FS_{rs}(\lambda) - \Delta, \quad (2)$$

where F is surface Fresnel reflectance and is 0.023 for our measurement geometry, and Δ is a corrector for residual surface-reflected light that was derived iteratively.²²

For the 2001 cruise, a Satlantic hyperspectral tethered spectral radiometer buoy (hyperTSRB) was used to obtain measurements for determining R_{rs} . This instrument operates in the range 400–1000 nm and measures the above-surface downwelling irradiance E_d and the near-surface upwelling radiance L_u . The L_u sensor is separated from the E_d sensor by 66 cm, meaning that, to calculate R_{rs} , L_u must be extrapolated through this subsurface layer (0.66 m from surface) and the air–sea interface to give the water-leaving radiance L_w . R_{rs} is then calculated from the ratio L_w/E_d . The method of Du *et al.*²³ was used to propagate the upwelling radiance, as the software provided with the TSRB instrument (ProSoft) was found less accurate in processing data of coastal

waters. No correction for TSRB self-shading was made.

B. Phytoplankton Absorption Coefficients and Cell Densities

Phytoplankton absorption spectra were measured from near-surface water samples, which were filtered under low pressure through a 25 mm diameter GF/F filter. Spectrophotometric determination of total, detrital, and phytoplankton pigment absorption was performed, and a filter pad path length amplification factor was calculated by the method of Lohrenz.²⁴ Cell densities of *K. brevis* were measured from near-surface water samples for each of the stations by use of an onboard Olympus CK-30 inverted microscope. A reference absorption spectrum for *Karenia brevis* required for SI analysis was obtained from filter pad absorption measurements of a *K. brevis* culture following the methods outlined above.

C. Inversion Methods

Phytoplankton absorption spectra were derived from inversions of *in situ* hyperspectral measurements of R_{rs} from the QAA of Lee *et al.*¹⁸ for optically deep

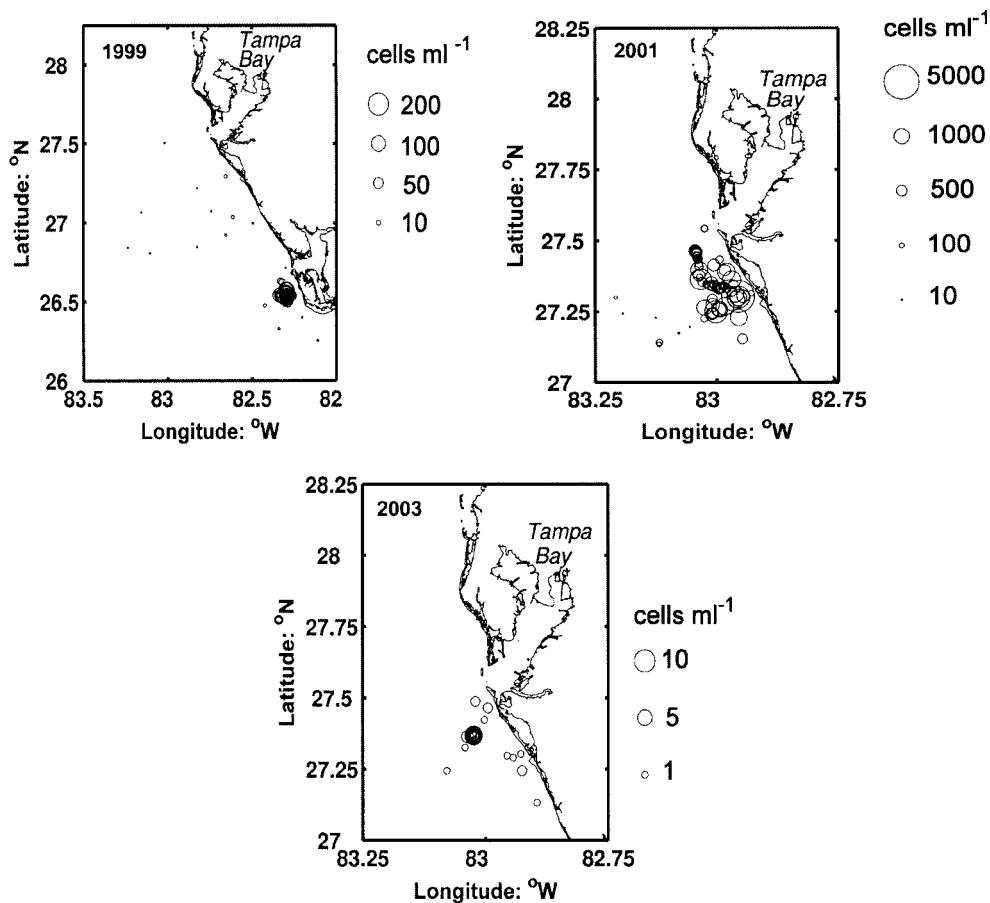


Fig. 1. ECOHAB area of study. Circles show surface cell densities of *K. brevis* for 9–14 September 1999, 20–25 October 2001, and 3–7 November 2003.

water. This algorithm has been shown to perform well in coastal waters¹⁸ and so is suitable for our area of study. Unlike semianalytical models, the QAA does not require a full spectral model for the phytoplankton absorption coefficient, a_{φ} , but instead allows $a_{\varphi}(\lambda)$ to be derived independently from $R_{rs}(\lambda)$. Its accuracy has been shown to be similar to that of optimization methods and its calculation efficiency similar to that of empirical algorithms,¹⁸ making it simple and quick to apply. Appendix A provides a description of the mathematical steps involved in the inversion process.

D. Similarity Index Analysis

Phytoplankton absorption spectra retrieved from remote sensing reflectance using the QAA, $a_{\varphi}^{Rrs}(\lambda)$, were compared to a *K. brevis* reference filter pad absorption spectrum, $a_{\varphi}^{ref}(\lambda)$, using a similarity index analysis as described by Millie *et al.*³ and Kirkpatrick *et al.*⁵ In brief, fourth-derivative spectra⁶ were computed from phytoplankton absorption spectra that have been normalized to their mean value of 400 to 700 nm.²⁵ Fourth derivatives are calculated to amplify spectral inflections and so to enhance detection of small spectral variations. Unique spectral inflections are found in *K. brevis* absorption spectra because of the presence of the photosynthetic pigment, gyroxanthin diester.³ The data are then transformed

by use of a normalized ratio method; i.e., each data pair is divided at every wavelength by the larger of the pair. The SI is computed from the angle between two vectors such that

$$SI = \frac{A_{ref} \cdot A_{Rrs}}{|A_{ref}| \times |A_{Rrs}|}, \quad (3)$$

where A_{ref} and A_{Rrs} are the vectors that comprise the fourth derivatives of the *K. brevis* reference filter pad absorption spectrum and the reflectance-derived phytoplankton absorption spectrum, respectively. The SI calculation yields a number from zero to one, where zero indicates no similarity between reference and derived spectra, and one indicates absolute similarity between reference and derived spectra.

E. Evaluation of QAA and SI under Different Water Conditions

We hypothesized that water constituents may have an effect on the efficacy of the QAA and the SI in detecting *K. brevis* blooms. Therefore a sensitivity analysis was conducted in which we tested the effects of variable cell and CDOM concentrations on QAA–SI detection of *K. brevis*. Cell concentration was chosen as a variable parameter in the sensitivity analysis to

permit us to examine the effect of the relative contribution of *K. brevis* to $R_{rs}(\lambda)$ on the performance of the QAA-SI; CDOM was chosen because its absorption in the blue overlaps strongly the phytoplankton absorption, and an analysis of the effect of its magnitude on QAA $\alpha_{\varphi}^{Rrs}(\lambda)$ retrieval and subsequent SI analysis seemed prudent. To implement the sensitivity analysis, we employed a combination of Mie and radiative transfer modeling (Hydrolight 4.1; see Ref. 26).

Mie modeling was used to calculate *K. brevis* inherent optical properties (IOPs) for a series of cell concentrations that ranged from 75 cells ml⁻¹ (low concentration) to 6190 cells ml⁻¹ (high concentration). This range was based on cell concentrations observed in the field and in the laboratory.²⁷ The Mie model was run by use of a modified code from Bohren and Huffman.²⁸ Inputs necessary for execution of the model included an assumed real refractive index for *K. brevis* of 1.053, a particle size distribution, and an optical thickness ρ' derived from Q_a , the absorption efficiency. ρ' is the product of the absorption coefficient of cell material and cell diameter,²⁹ and we estimated it by initially determining single-cell absorption efficiency $Q_a(\lambda)$, using microphotometry.³⁰ We then estimated ρ' by using the equation solver in Microsoft Excel to determine the best ρ' for the following equation³¹:

$$Q_a(\lambda) = 1 + \frac{\{2 \exp[-\rho'(\lambda)]\}}{\rho'(\lambda)} + \frac{2\{\exp[-\rho'(\lambda)] - 1\}}{\rho'(\lambda)}. \quad (4)$$

Note that absorption coefficient a is equal to 4π times the imaginary component of refractive index divided by wavelength.³²

All above parameters were obtained from laboratory measurements made on a monospecific culture of *K. brevis*.²⁷ The output from the model provided *K. brevis* total absorption a , total scattering b , and backscattering b_b , at 5 nm resolution for each of the cell concentrations.

The Hydrolight radiative transfer model computes radiance distributions and related quantities in the ocean.²⁶ In our study, it was used to predict $R_{rs}(\lambda)$ for variable cell densities and CDOM concentrations. The Hydrolight model allows the user to provide input files that define the IOPs used in a simulation. Results from the Mie model were used to construct these IOP input files in the following manner: Total absorption was calculated from the sum of Mie modeled *K. brevis* absorption, and absorption that was due to CDOM, a_{CDOM} . a_{CDOM} was modeled from the expression³³

$$a_{CDOM} = a_{CDOM}(\lambda_0) \exp[-\gamma(\lambda - \lambda_0)], \quad (5)$$

where $\lambda_0 = 440$ nm and where the spectral slope, γ , was chosen to be 0.019 nm⁻¹ based on *in situ* observations.²⁷ Note that γ is the spectral slope for CDOM only, not for CDOM and detritus as in the spectral

slope, S_{QAA} , used in the QAA. The total particulate scattering, b_p , was given by the Mie model and used to derive the beam attenuation coefficient, $c (=a + b)$. We obtained total backscattering coefficients (b_b) by adding Mie modeled particulate backscattering, b_{bp} , to half of the scattering coefficients of pure water, b_w ,³²

$$b_b = b_{bp} + 0.5b_w, \quad (6)$$

and b_w values were interpolated from Table 3 of Mobley.³²

Hydrolight was set to run with inelastic scattering (Raman, chlorophyll, and CDOM fluorescence) included. As chlorophyll fluorescence was selected to be included in the simulations, it was necessary to ensure that the chlorophyll concentration was consistent with the specific absorption defined in the run. Therefore, chlorophyll concentration [Chl] was derived by use of the Mie modeled *K. brevis* absorption at 675 nm from

$$[\text{Chl}] = a_{675}/a_{675}^*, \quad (7)$$

where a_{675}^* is the chlorophyll a specific absorption measured in the laboratory.²⁷ Hydrolight requires that CDOM concentration be defined by the user if inelastic scattering processes are included in simulations. Therefore the absorption of CDOM at 440 nm was user defined (see below), and its spectral slope γ was set to 0.019 nm⁻¹. Both chlorophyll and CDOM concentrations were assumed to be homogeneous with depth for all simulations. Latitude, longitude, and time of day were chosen to be representative of field observations.

Two Hydrolight scenarios were modeled: In scenario I, CDOM absorption at 440 nm, $a_{CDOM}(440)$, was held constant at 0.25 m⁻¹, and input IOPs were allowed to vary. We achieved this by successively feeding Hydrolight input files constructed from the Mie modeled IOPs for each of the cell concentrations (0–6190 cells ml⁻¹). In scenario II, input IOPs were held constant by use of the Mie modeled IOPs for a cell concentration of 6190 cells ml⁻¹, and $a_{CDOM}(440)$ was allowed to vary from 0 to 3.0 m⁻¹. This range of CDOM absorption values was intended to encompass both realistic ranges observed in the field²⁷ and extreme values.

3. Results and Discussion

A. *In Situ* Data

Figure 2 shows remote sensing reflectance, $R_{rs}(\lambda)$, measured during three separate ECOHAB cruises. R_{rs} showed considerable variability in both spectral shape and magnitude from year to year, indicating the different water types encountered during each cruise. Measurements made of water samples also showed a high degree of variability [Fig. 3(a)]. Note that analyses of filter pads were not complete for all stations; therefore only a subset of stations is shown

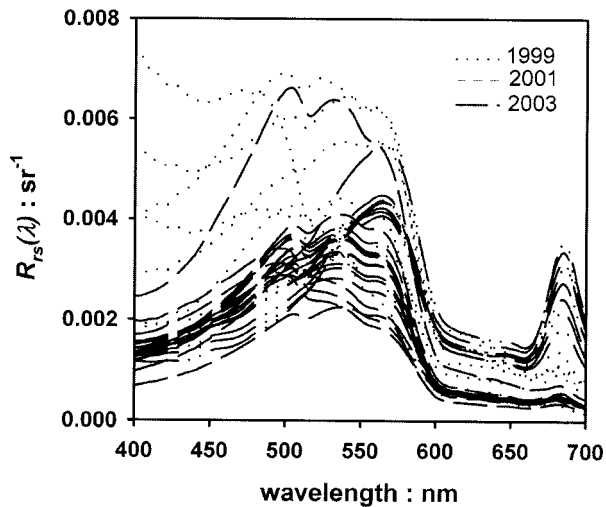


Fig. 2. *In situ* hyperspectral measurements of remote sensing reflectance, $R_{rs}(\lambda)$, for 9–14 September 1999, 20–25 October 2001, and 3–7 November 2003.

in Fig. 3. Phytoplankton absorption spectra were retrieved from these data by application of the algorithm of Lee *et al.*¹⁸ [Fig. 3(b)]. Only data in the range 400–560 nm are shown because, beyond these wavelengths, there is not sufficient information to reliably derive a_ϕ from R_{rs} owing to the strong absorption by

water molecules.³⁴ Reflectance-derived a_ϕ spectra, $a_\phi^{Rrs}(\lambda)$, were compared with filter pad a_ϕ spectra, $a_\phi^{pad}(\lambda)$, at selected wavelengths [Fig. 3(c)]. Following the analysis of Lee and Carder,³⁴ the R^2 value and the percentage difference between these two data sets were calculated. The percentage difference is defined as

$$\% \text{ difference} = \frac{\{\text{mean}[a_\phi^{pad}(\lambda) - a_\phi^{Rrs}(\lambda)]^2\}^{1/2}}{\text{mean}[a_\phi(\lambda)^{pad}]} \times 100\%. \quad (8)$$

An R^2 value of 0.891 and a mean percentage difference of 22.8% were obtained, confirming that the two data sets agree reasonably well. As in Lee and Carder's³⁴ estimation of errors, it is unclear what contributes most to the difference between $a_\phi^{pad}(\lambda)$ and $a_\phi^{Rrs}(\lambda)$. There is an error associated with the filter pad measurements that is due to path length amplification and variable sample loading of the filter pad.²⁴ In the QAA, various parameters are assumed, empirically estimated, or modeled and cannot be considered error free.³⁴ One example of an assumed value is the constant S_{QAA} value of 0.015 nm^{-1} used for all cruises and all stations. Theoretically, a different S_{QAA} value should be used for each station to allow

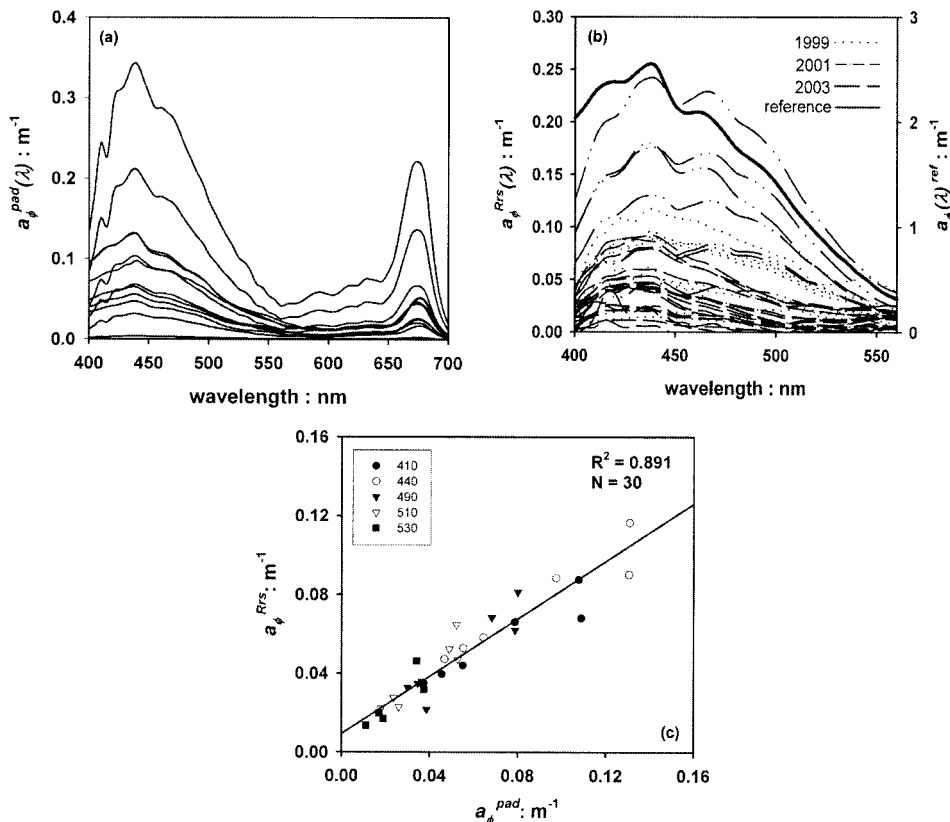


Fig. 3. (a) Phytoplankton absorption spectra measured from filter pads, $a_\phi^{pad}(\lambda)$, for a subset of ECOHAB stations. (b) Reflectance-derived phytoplankton absorption spectra, $a_\phi^{Rrs}(\lambda)$, for 9–14 September 1999, 20–25 October 2001, and 3–7 November 2003. The reference, $a_\phi^{ref}(\lambda)$, is an absorption spectrum determined from filter pad measurements of a monospecific culture of *K. brevis*. (c) Filter pad measured phytoplankton absorption, a_ϕ^{pad} , compared with reflectance-derived phytoplankton absorption a_ϕ^{Rrs} , at selected wavelengths.

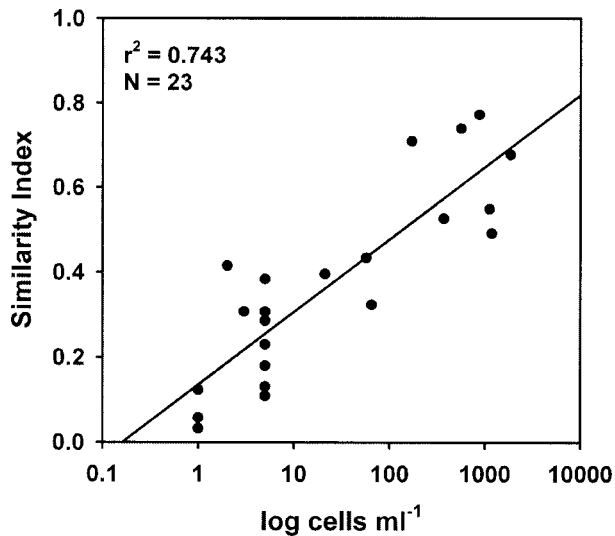


Fig. 4. Surface *K. brevis* cell concentration versus SI magnitude.

the most accurate retrieval of $a_{\varphi}^{Rrs}(\lambda)$.^{18,34} Another source of difference may lie in the fact that filter pad measurements sample only a discrete volume of water, whereas $a_{\varphi}^{Rrs}(\lambda)$ spectra represent the properties of the upper water column.³⁴ It is difficult to quantitatively state what the errors in R_{rs} are, and this is a matter for ongoing research. Errors in R_{rs} will most likely affect the spectral amplitude and not the spectral shape.³⁵ For our purposes, spectral shape is far more important than absolute spectral amplitude because the fourth derivative in the SI is sensitive to spectral inflections. It is this sensitivity that permits discrimination of *K. brevis*.

Figures 1(a)–1(c) present plots of surface *K. brevis* cell density as determined by microscopic enumeration for each of the three years. The greatest surface cell abundance was encountered during the September 2001 cruise, with cell densities in excess of 1000 cells ml^{-1} . Concentrations in this range are classified as a medium bloom³⁶ and may cause respiratory irritation and isolated fish kills. The lowest cell densities were observed in November 2003, where surface concentrations reached just 7 cells ml^{-1} .

A similarity index was calculated for $a_{\varphi}^{Rrs}(\lambda)$ and a *K. brevis* reference spectrum as described in Subsection 2.4. The magnitude of the similarity index was then compared to surface cell counts (Fig. 4). A strong correlation between the two parameters was observed with an R^2 value of 0.743. This is in agreement with Kirkpatrick *et al.*,⁵ who also found a significant correlation between the similarity index and *K. brevis* biomass and points to the potential use of the SI as an indication of bloom strength.

The analyses described above were repeated with S_{QAA} changed from the value of 0.015 to 0.019 nm^{-1} of Lee *et al.*,¹⁸ in an attempt to be consistent with γ values used in our modeling work (Subsection 2.5). It was found that, with $S_{QAA} = 0.019 \text{ nm}^{-1}$, the R^2 value for $a_{\varphi}^{pad}(\lambda)$ versus $a_{\varphi}^{Rrs}(\lambda)$ decreased to 0.761, the

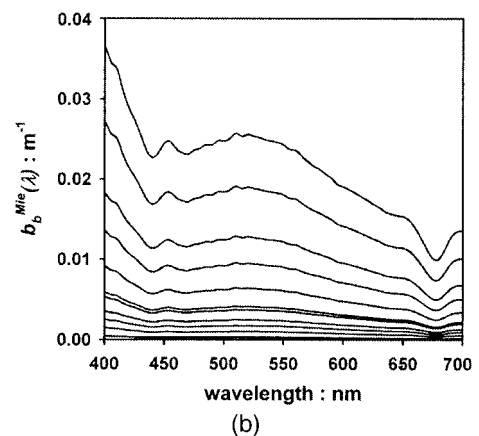
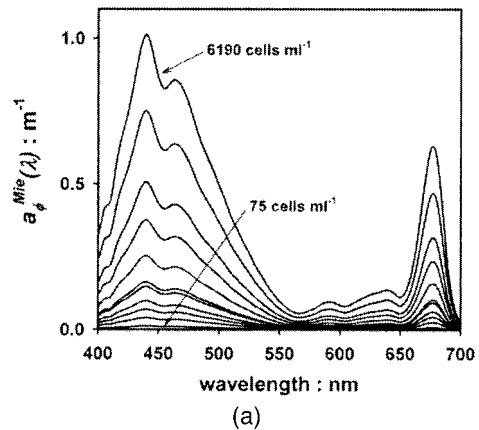


Fig. 5. Mie modeled (a) absorption spectra, $a_{\varphi}^{\text{Mie}}(\lambda)$, and (b) backscattering spectra, $b_b^{\text{Mie}}(\lambda)$, for cell concentrations in the range 75–6190 cells ml^{-1} .

mean percentage difference increased to 34.3%, and the R^2 for cell concentration versus SI decreased to 0.739. It is probable that 0.015 nm^{-1} was, on average, a better representation of the water types that we sampled during the three cruises and so produced more satisfactory results.

B. Simulated Data

Figures 5(a) and 5(b) show the Mie modeled hyperspectral absorption and backscattering coefficients used to construct Hydrolight input IOP files in simulations of R_{rs} . The results of these simulations are shown in Figs. 6 and 7. Figure 6(a) shows scenario I, in which $a_{\text{CDOM}}(440)$ was held constant at 0.25 m^{-1} and input IOPs, calculated from a range of cell concentrations from 75 to 6190 cells ml^{-1} , varied. As cell concentration increases from low to high values, the magnitude of R_{rs} at longer wavelengths increases and becomes more peaked near 562 and 688 nm. The shape of the peak centered about 562 nm is due to the removal of photons in the blue by chlorophyll and accessory pigments and in the red by chlorophyll. The increase in spectra magnitude may be explained by increased backscattering as cell concentrations rise. No sediments were included in these Hydrolight runs, so scattering is due only to water itself and to

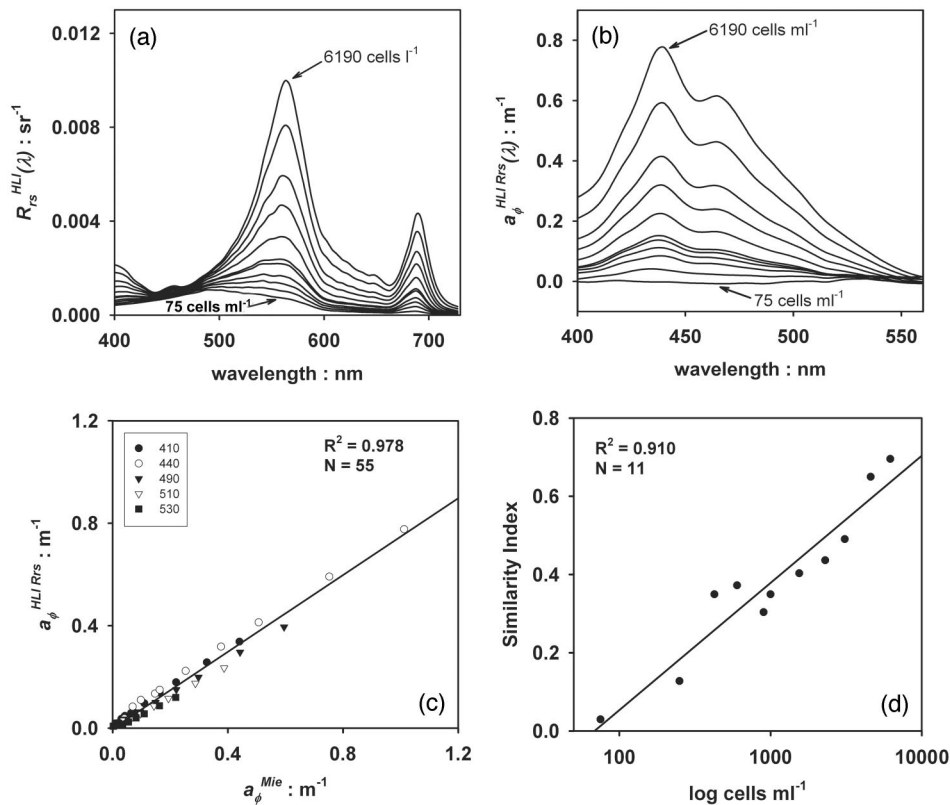


Fig. 6. (a) Scenario I Hydrolight simulation of remote sensing reflectance, $R_{rs}^{HLI}(\lambda)$. CDOM absorption is held constant at $0.25\ m^{-1}$, and input IOPs, calculated from a range of cell concentrations from 75 to 6190 $cells\ ml^{-1}$, are varied. (b) Scenario I reflectance-derived phytoplankton absorption, $a_{\phi}^{HLI Rrs}(\lambda)$, for cell concentrations ranging from 75 to 6190 $cells\ ml^{-1}$. (c) Mie modeled phytoplankton absorption, a_{ϕ}^{Mie} , compared with reflectance-derived phytoplankton absorption, $a_{\phi}^{HLI Rrs}$, at selected wavelengths for scenario I simulations. (d) *K. brevis* cell concentration versus similarity index magnitude for scenario I simulations.

the *K. brevis* cells (scattering of CDOM is negligible³²). The 688 nm peak is due to chlorophyll fluorescence, the magnitude of which increases as cell concentration increases.

Figure 6(b) shows phytoplankton absorption spectra derived from scenario I Hydrolight simulations of remote sensing reflectance, $a_{\phi}^{HLI Rrs}(\lambda)$. For the simulations using IOPs from the lowest cell concentration (75 $cells\ ml^{-1}$), $a_{\phi}^{HLI Rrs}$ is not successfully derived and is negative. This is due to the relatively small contribution of *K. brevis* to R_{rs} at these low concentrations. However, at cell concentrations above 75 $cells\ ml^{-1}$ (low category bloom³⁵), the QAA derives positive values for $a_{\phi}^{HLI Rrs}$. To give an indication of how well $a_{\phi}^{HLI Rrs}$ values agree with the a_{ϕ}^{Mie} values, the percentage difference between these two values was calculated for each cell concentration as in Eq. (8) for a wavelength range of 400–560 nm. However, in this case $a_{\phi}^{Mie}(\lambda)$ is used in place of $a_{\phi}^{pad}(\lambda)$. The percentage difference, excluding the 75 $cells\ ml^{-1}$ concentration, which produced negative $a_{\phi}^{HLI Rrs}$ values, ranged from 16.1% to 33.4% (Table 2), with an average of 27.4%. The R^2 value for a regression of selected wavelengths of a_{ϕ}^{Mie} values against $a_{\phi}^{HLI Rrs}$ values, at all the cell concentrations used, was found to be 0.978 [Fig. 6(c)], showing that the QAA performs well in

retrieving the absorption properties that were used to simulate $R_{rs}(\lambda)$.

Initially, the QAA was implemented with ζ calculated as detailed in Appendix A. However, this was found to give less satisfactory $a_{\phi}^{HLI Rrs}$ retrievals and reduced the R^2 for a_{ϕ}^{Mie} versus $a_{\phi}^{HLI Rrs}$ to 0.874 (data not shown). The calculation of Lee *et al.*¹⁸ of ζ is empirical and based on the field data of Lee *et al.*²¹ These field data contain information for natural populations of phytoplankton, whereas our absorption data were modeled for a monospecific population of *K. brevis*. Better agreement between a_{ϕ}^{Mie} and $a_{\phi}^{HLI Rrs}$ values was achieved by use of an average ζ value equal to the average $a_{\phi}^{Mie}(410)/a_{\phi}^{Mie}(440)$ ratio over all the cell concentrations.

Cell concentration is plotted against SI in Fig. 6(d). For these modeled data, an R^2 of 0.910 was obtained, showing a strong relationship between similarity index magnitude and surface cell concentration, also observed by Kirkpatrick *et al.*⁵ and indicating the potential utility of the SI in making approximate estimations of bloom strength.

Figure 7(a) shows scenario II Hydrolight simulations of R_{rs} in which $a_{CDOM}(440)$ was varied from 0 to $3.0\ m^{-1}$ and input IOPs, corresponding to a cell concentration of 6190 $cells\ ml^{-1}$, held constant. The

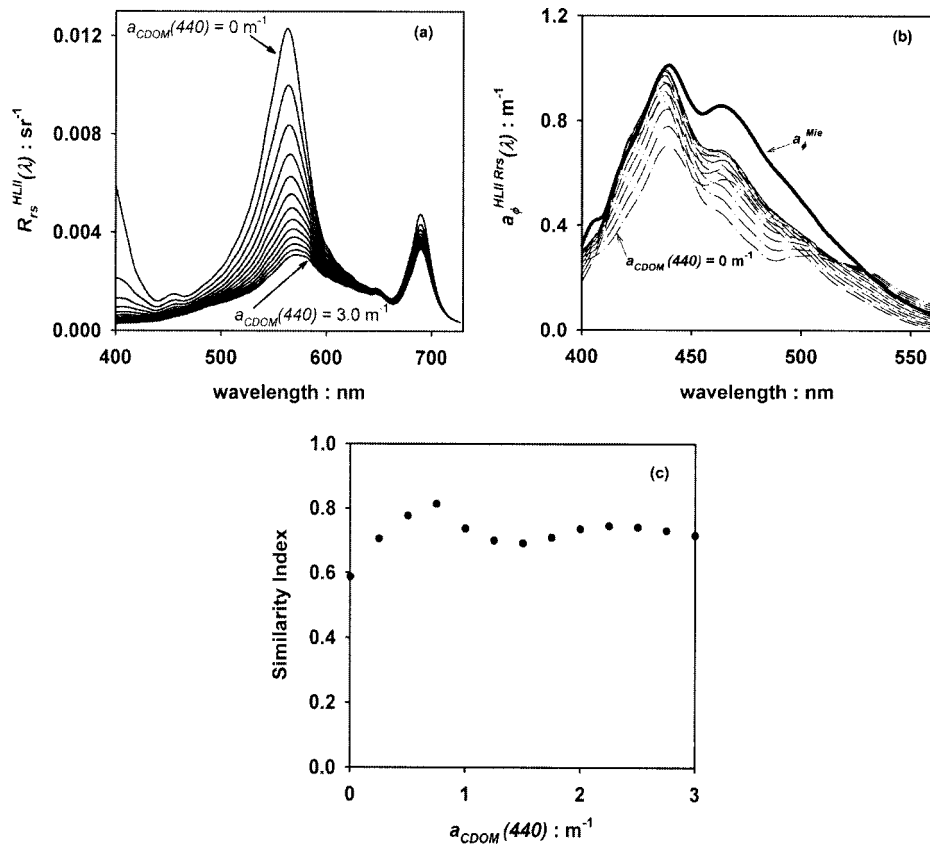


Fig. 7. (a) Scenario II Hydrolight simulation of remote sensing reflectance, $R_{rs}^{HLII}(\lambda)$. The CDOM absorption is varied from 0 to 3.0 m^{-1} , and IOPs corresponding to a cell concentration of 6190 cells ml^{-1} are held constant. (b) Scenario II reflectance-derived phytoplankton absorption, $a_{\phi}^{HLII Rrs}$, for CDOM absorption ranging from 0 to 3.0 m^{-1} and a constant cell concentration of 6190 cells ml^{-1} . (c) CDOM absorption at 440 nm, $a_{CDOM}(440)$, versus similarity index magnitude.

overall shape of the spectra is similar to that of scenario I spectra, with two peaks centered around 562 and 688 nm. However, in this case there is an inverse relationship between the magnitude of the R_{rs} spectra and CDOM absorption. Increasing levels of CDOM are seen to influence the magnitude of the 562 nm peak the most, with the red fluorescence peak showing much less variation. The green peak becomes slightly redshifted at the higher CDOM absorption

values owing to the removal of more photons in the green region at these higher concentrations.

Phytoplankton absorption spectra derived from scenario II Hydrolight simulations of remote sensing reflectance, $a_{\phi}^{HLII Rrs}(\lambda)$, are shown in Fig. 7(b). The solid curve is $a_{\phi}^{Mie}(\lambda)$ calculated at a cell concentration of 6190 cells ml^{-1} and was used to construct the input IOP files for Hydrolight. Despite the fact that inputs IOPs were held constant in these simulations, $a_{\phi}^{HLII Rrs}(\lambda)$ spectra that differ in both shape and magnitude are derived for each CDOM absorption value. The discrepancy between $a_{\phi}^{HLII Rrs}(\lambda)$ and $a_{\phi}^{Mie}(\lambda)$ is greatest in the 450–530 nm spectral region and is most likely due to a mismatch between the particulate backscattering spectral shape, $b_{bp}(\lambda)$, used in the QAA, and $b_{bp}(\lambda)$ for *K. brevis*. In the QAA, $b_{bp}(\lambda)$ is a smooth monotonic function of wavelength, but the Mie modeled $b_{bp}(\lambda)$ is not, especially at the high cell concentration used (6190 cells ml^{-1}). This fact should not seriously affect the efficacy of the SI since the fourth derivative depends more on the spectral shape of a_{ϕ} , especially around inflections, and less on the actual values.³⁵

The relationship between $a_{CDOM}(440)$ and the similarity index is shown in Fig. 7(c). A minimum index of similarity of 0.58 is obtained for $a_{CDOM}(440) = 0 m^{-1}$ and a maximum index of similarity of 0.86 for

Table 2. Cell Concentrations and Percentage Difference between a_{ϕ}^{Mie} Values and $a_{\phi}^{Rrs HLII}$ Values in the Range 400–560 nm^a

Cell Concentration: Cells ml^{-1}	% Difference
75	177.9
250	33.4
425	21.5
600	16.1
900	28.0
1000	27.3
1550	26.9
2300	28.0
3100	29.7
4600	31.3
6190	32.6

^aThe average percentage difference, excluding the 75 cells ml^{-1} concentration, which derived negative $a_{\phi}^{HLII Rrs}$ values, was 27.4%.

$a_{\text{CDOM}}(440) = 0.75 \text{ m}^{-1}$. $a_{\text{CDOM}}(440) = 0 \text{ m}^{-1}$ gives the lowest index of similarity, because a CDOM + detritus absorption term is explicit in the QAA's calculation of a_{φ} ($= a - a_g - a_w$). Subtracting a_g from reflectance-derived a that includes no contribution from CDOM will result in an underestimation of a_{φ} , especially in the blue region of the spectrum where CDOM absorption is largest [Fig. 7(b)].

4. Summary

Based on studies of its absorption properties, we have postulated that *Karenia brevis* would give rise to optical signatures in hyperspectral remote sensing reflectance that are sufficiently unique to allow its exploitation for detection and assessment of blooms. To explore this hypothesis, *in situ* hyperspectral remote sensing reflectance data, collected during three bloom seasons (during the years 1999, 2001, and 2003) and covering a wide range of water conditions in the northern Gulf of Mexico, were examined. We applied the quasi-analytical inversion algorithm of Lee *et al.*¹⁸ to these data to derive phytoplankton absorption coefficients, and it was found to agree well with phytoplankton absorption measured on filter pads, with an average percentage difference of 22.8% and an R^2 value of 0.891. A strong relationship was found between cell concentration and SI ($R^2 = 0.743$), showing the potential utility of the SI as an indicator of bloom strength.

To explore the effect of varying the levels of cell concentration and CDOM absorption on the efficacy of the QAA and SI to detect blooms, we undertook a combination of Mie and radiative transfer modeling to simulate two water column scenarios: scenario I, in which CDOM absorption was held constant and the cell concentration was varied, and scenario II, in which CDOM absorption was varied and the cell concentration was held constant.

Scenario I simulations found that the QAA was unable to derive a_{φ} at a concentration of 75 cells ml^{-1} , mostly because of the relatively small contribution of *K. brevis* to R_{rs} . A regression of a_{φ}^{Mie} values against a_{φ}^{Rrs} values, for selected wavelengths, gave an R^2 of 0.978, and the average percentage difference between the two was found to be 27.4%. In agreement with the *in situ* data, a strong correlation between cell concentration and SI magnitude was observed ($R^2 = 0.910$).

Scenario II simulations revealed that CDOM absorption has an effect on $a_{\varphi}^{\text{HLII Rrs}}$ with a different $a_{\varphi}^{\text{HLII Rrs}}$ spectrum derived for each CDOM absorption value, despite constant *K. brevis* cell concentration. Both the magnitude and the shape of the reflectance-derived $a_{\varphi}^{\text{HLII Rrs}}$ spectra were observed to differ from the a_{φ}^{Mie} spectra, with differences in magnitude especially evident in the 440–530 nm region and most likely due to differences in the $b_{\text{bp}}(\lambda)$ used in the QAA and in that predicted by Mie modeling.

Analysis of both *in situ* and simulated data revealed that the spectral slope, S_{QAA} , and phytoplankton absorption properties in the blue region of the

spectrum, ζ , are two parameters that should be considered with care; according to Lee *et al.*,¹⁸ region-specific information on these properties will improve a_{φ}^{Rrs} retrievals.

These results suggest that regional-scale detection and mapping of *Karenia brevis* blooms based on hyperspectral measurements of remote-sensing reflectance appear to be feasible. These methods may be used to complement and enhance monitoring and management programs already in place that utilize *in situ* detection methods, e.g., the *Brevebuster*. Our results have been based on *in situ* measurements of R_{rs} , but it should be possible to extend these techniques to aircraft and satellite measurements of R_{rs} , and future work will include an exploration of this possibility.

Appendix A

The first step of the QAA is to calculate remote sensing reflectance below the surface, r_{rs} , from

$$r_{\text{rs}} = \frac{R_{\text{rs}}}{0.52 + 1.7R_{\text{rs}}}. \quad (\text{A1})$$

r_{rs} is a measure of the ratio, u , of the backscattering coefficient, b_b , to the sum of absorption, a , and backscattering coefficients, where³⁷

$$u = \frac{b_b}{a + b_b}. \quad (\text{A2})$$

u may be derived from r_{rs} as by Gordon *et al.*³⁷:

$$r_{\text{rs}}(\lambda) = g_0 u(\lambda) + g_1 [u(\lambda)]^2. \quad (\text{A3})$$

g_0 and g_1 must be predetermined, and Lee *et al.*¹⁸ took the average of the oceanic case 1 values of Gordon *et al.*³⁷ and the coastal water values of Lee *et al.*³⁸ to give $g_0 = 0.0895$ and $g_1 = 0.1247$. From Eq. (3),¹⁸

$$u(\lambda) = \frac{-g_0 + [(g_0)^2 + 4g_1 r_{\text{rs}}(\lambda)]^{1/2}}{2g_1}. \quad (\text{A4})$$

The QAA then empirically estimates the total absorption coefficient at a reference wavelength, λ_0 , where R_{rs} can be well measured: 555, or 650 nm for more turbid waters:

$$a(\lambda_0) = 0.0596 + 0.2[a(440)_i - 0.01], \quad (\text{A5})$$

where

$$a(440)_i = \exp(-0.62 - 1.97\rho + 0.79\rho^2), \quad (\text{A6})$$

$$\rho = \ln \frac{r_{\text{rs}}(440)}{r_{\text{rs}}(555)}. \quad (\text{A7})$$

Knowing $a(\lambda_0)$ then allows an analytical calculation of the particulate backscattering coefficient at the

reference wavelength, $b_{bp}(\lambda_0)$, from r_{rs} :

$$b_{bp}(\lambda_0) = \frac{u(\lambda_0)\alpha(\lambda_0)}{1 - u(\lambda_0)} - b_{bw}(\lambda_0). \quad (A8)$$

The spectral power, Y , for $b_{bp}(\lambda)$ is empirically estimated from

$$Y = 2.2 \left\{ 1 - 1.2 \exp \left[-0.9 \frac{r_{rs}(440)}{r_{rs}(555)} \right] \right\} \quad (A9)$$

and the particulate backscattering spectrum, $b_{bp}(\lambda)$, derived from

$$b_{bp}(\lambda) = b_{bp}(\lambda_0)(\lambda_0/\lambda)^Y. \quad (A10)$$

The total absorption, $\alpha(\lambda)$, is then calculated by substituting $b_{bp}(\lambda)$ values into

$$\alpha(\lambda) = \frac{[1 - u(\lambda)][b_{bw}(\lambda) + b_{bp}(\lambda)]}{u(\lambda)}. \quad (A11)$$

The QAA calculates absorption by detritus and gelbstoff, α_g : It does not allow separation of the two:

$$\alpha_g(440) = \frac{[\alpha(410) - \zeta\alpha(440)]}{\xi - \zeta} - \frac{[\alpha_w(410) - \zeta\alpha_w(440)]}{\xi - \zeta}, \quad (A12)$$

$$\alpha_g(\lambda) = \alpha(440)\exp[-S_{QAA}(\lambda - 440)], \quad (A13)$$

where

$$\zeta = \frac{\alpha_\varphi(410)}{\alpha_\varphi(440)} = 0.71 + \frac{0.06}{0.8 + r_{rs}(440)/r_{rs}(555)}, \quad (A14)$$

$$\xi = \frac{\alpha_g(410)}{\alpha_g(440)} = \exp[S(440 - 410)]. \quad (A15)$$

Absorption by phytoplankton pigments is then given by

$$\alpha_\varphi^{Rrs} = \alpha - \alpha_g - \alpha_w. \quad (A16)$$

We are very grateful for the comments and suggestions provided by our two anonymous reviewers. This research was supported by funding from the Office of Naval Research (N000140310896) and by NASA (NNG04GA02G).

References

1. D. M. Anderson, P. Hoagland, Y. Kaoru, and A. W. White (2000), "Economic impacts from harmful algal blooms (HABs) in the United States," Tech. Rep. WHOI-2000-11 (Woods Hole Oceanographic Institution, 2000).
2. P. A. Tester and K. A. Steidinger, "Gymnodinium breve red tide

- blooms: initiation, transport and consequences of surface circulation," *Limnol. Oceanogr.* **42**, 1039–1051 (1997).
3. D. F. Millie, O. M. Schofield, G. J. Kirkpatrick, G. Johnsen, P. A. Tester, and B. T. Vinyard, "Detection of harmful algal blooms using photopigments and absorption signatures: a case study of the Florida red tide dinoflagellate, *Gymnodinium breve*," *Limnol. Oceanogr.* **42**, 1240–1251 (1997).
4. O. M. Schofield, J. Grzymiski, W. P. Bissett, G. J. Kirkpatrick, D. F. Millie, M. Moline, and C. S. Roesler, "Optical monitoring and forecasting systems for harmful algal blooms: possibility or pipe dream?" *J. Phycol.* **35**, 1477–1496 (1999).
5. G. J. Kirkpatrick, O. M. Schofield, D. F. Millie, and M. Moline, "Optical discrimination of a phytoplankton species in natural mixed populations," *Limnol. Oceanogr.* **45**, 467–471 (2000).
6. W. L. Butler and D. W. Hopkins, "An analysis of fourth derivative spectra," *Photochem. Photobiol.* **12**, 451–456 (1970).
7. E. B. Órnólfssdóttir, J. L. Pinckney, and P. A. Tester, "Quantification of the relative abundance of the toxic dinoflagellate, *Kareia brevis* (Dinophyta), using unique photopigments," *J. Phycol.* **39**, 449–457 (2003).
8. G. J. Kirkpatrick, C. Orrico, M. A. Moline, M. Oliver, and O. M. Schofield, "Continuous hyperspectral absorption measurements of colored dissolved organic material in aquatic systems," *Appl. Opt.* **42**, 6564–6568 (2003).
9. G. J. Kirkpatrick, J. Hillier, and C. Boyes, "BreveBuster results from the channel marker at the mouth of Charlotte Harbor," [http://isurus.mote.org/~jhilier/Phytoplankton Ecology/WebDisplay/Display.html](http://isurus.mote.org/~jhilier/Phytoplankton_Ecology/WebDisplay/Display.html).
10. O. Schofield, R. Chant, J. Kohut, and S. Glenn, "The growth of the New Jersey Shelf Observing System for monitoring plumes and blooms on the Mid-Atlantic continental shelf," presented at OCEANS 2004, Kobe, Japan, 9–12 November 2004.
11. J. J. Cullen, A. M. Ciotti, R. F. Davis, and M. R. Lewis, "Optical detection and assessment of algal blooms," *Limnol. Oceanogr.* **42**, 1223–1239 (1997).
12. P. A. Tester and R. P. Stumpf, "Phytoplankton blooms and remote sensing: what is the potential for early warning?" *J. Shellfish Res.* **17**, 1469–1471 (1998).
13. R. P. Stumpf, M. E. Culver, P. A. Tester, M. Tomlinson, G. J. Kirkpatrick, B. A. Pederson, E. Truby, V. Ransibrahmanakul, and M. Soracco, "Monitoring *Karenia brevis* blooms in the Gulf of Mexico using satellite ocean color imagery and other data," *Harmful Algae* **2**, 147–160 (2003).
14. D. G. Thomas, "The use of SeaWiFS-derived bio-optical properties to characterize harmful algal blooms," M.Sc. thesis (University of Southern Mississippi, 2000).
15. R. P. Stumpf, "Applications of satellite ocean color sensors for monitoring and predicting harmful algal blooms," *Human Ecol. Risk Assess.* **7**, 1363–1368 (2001).
16. M. C. Tomlinson, R. P. Stumpf, V. Ransibrahmanakul, E. W. Truby, G. J. Kirkpatrick, B. A. Pederson, G. A. Vargo, and C. A. Heil, "Evaluation of the use of SeaWiFS imagery for detecting *Karenia brevis* harmful algal blooms in the eastern Gulf of Mexico," *Remote Sens. Env.* **91**, 293–303 (2004).
17. J. P. Cannizzaro, K. L. Carder, F. R. Chen, J. J. Walsh, Z. Lee, C. Heil, and T. Villareal, "A novel optical classification technique for detection of red tides in the Gulf of Mexico: application to the 2001–2002 bloom event," in *Proceedings of Xth Annual Conference on Harmful Algae* (Florida Fish and Wildlife Conservation Commission of UNESCO, 2002), p. 43.
18. Z. P. Lee, K. L. Carder, and R. A. Arnone, "Deriving inherent optical properties from water color: a multiband quasi-analytical algorithm for optically deep waters," *Appl. Opt.* **41**, 5755–5772 (2002).
19. D. F. Millie, O. M. Schofield, G. J. Kirkpatrick, G. Johnsen, and T. J. Evens, "Using absorbance and fluorescence spectra to discriminate microalgae," *Eur. J. Phycol.* **37**, 313–322 (2002).
20. P. A. Staer and J. J. Cullen, "Detection of *Karenia mikimotoi* by

- spectral absorption signatures,” *J. Plank. Res.* **25**, 1237–1249 (2003).
21. Z. P. Lee, K. L. Carder, R. G. Steward, P. G. Peacock, C. O. Davis, and J. S. Patch, “An empirical algorithm for light absorption by ocean water based on color,” *J. Geophys. Res.* **130**, 27,976–27,978 (1998).
 22. Z. P. Lee, K. L. Carder, T. G. Peacock, C. O. Davis, and J. L. Mueller, “Method to derive ocean absorption coefficients from remote-sensing reflectance,” *Appl. Opt.* **35**, 453–462 (1996).
 23. K. P. Du, M. X. He, Z. P. Lee, and P. Chen, “A new data processing method for the Satlantic hyper-TSRB,” presented at Ocean Optics XVI (Santa Fe, N. Mex., November 18–22 2002), available on CD-ROM from Society of Photo-optical Instrumentation Engineers (SPIE).
 24. S. E. Lohrenz, “A novel theoretical approach to correct for pathlength amplification and variable sample loading in measurements of particulate spectral absorption by the quantitative filter technique,” *J. Plank. Res.* **22**, 639–657 (2000).
 25. C. S. Roesler, M. J. Perry, and K. L. Carder, “Modeling *in situ* phytoplankton absorption from total absorption spectra in productive inland marine waters,” *Limnol. Oceanogr.* **34**, 1510–1523 (1989).
 26. C. D. Mobley and L. K. Sundman, “Hydrolight 4.1 technical documentation,” Sequoia Scientific Bellevue, WA (2000).
 27. K. L. Mahoney, “Backscattering of light by *Karenia brevis* and implications for optical detection and monitoring,” Ph.D. dissertation (University of Southern Mississippi, 2003).
 28. C. F. Bohren and D. R. Huffman, *Absorption and Scattering of Light by Small Particles* (Wiley, 1983).
 29. H. C. van de Hulst, *Light Scattering by Small Particles* (Dover, 1981).
 30. G. L. Fahnenstiel, National Oceanic and Atmospheric Administration/Great Lakes Environmental Research Laboratory (NOAA/GLERL), Lake Michigan Field Station, 1431 Beach Streets Muskegon, Michigan 49441 (personal communication, 2001).
 31. A. Morel and A. Bricaud, “Theoretical results concerning light absorption in a discrete medium an application to specific absorption of phytoplankton,” *Deep Sea Res.* **28**, 1375–1393 (1981).
 32. C. D. Mobley, *Light and Water: Radiative Transfer in Natural Waters* (Academic, 1994).
 33. A. Bricaud, M. Babin, A. Morel, and H. Claustre, “Variability in the chlorophyll-specific absorption coefficients of natural phytoplankton: analysis and parameterization,” *J. Geophys. Res.* **100**, 13,321–13,332 (1995).
 34. Z. P. Lee and K. L. Carder, “Absorption spectrum of phytoplankton pigments derived from hyperspectral remote sensing reflectance,” *Remote Sens. Environ.* **89**, 361–368 (2004).
 35. Z. P. Lee, Naval Research Laboratory, Stennis Space Center, MS 39529 (personal communication, 2006).
 36. Florida Marine Research Institute, “Red tides in Florida, 1954–1998: Harmful Algal Bloom Historical Database” (CD-ROM, Version 1.0, 2001).
 37. H. R. Gordon, O. B. Brown, R. H. Evans, J. W. Brown, R. C. Smith, K. S. Baker, and D. K. Clark, “A semi-analytical radiance model of ocean color,” *J. Geophys. Res.* **93**, 10,909–10,924 (1988).
 38. Z. P. Lee, K. L. Carder, C. D. Mobley, R. G. Steward, and J. S. Patch, “Hyperspectral remote sensing for shallow waters. 2. Deriving bottom depths and water properties by optimization,” *Appl. Opt.* **38**, 3831–3843 (1999).